

Article

Assessment and Improvement of Melt Quality of Recycled Secondary A357 Alloy by Application of the High Shear Melt Conditioning (HSMC) Technology

Zhichao Niu, Zhongping Que ^{*}, Jayesh B. Patel  and Zhongyun Fan 

Brunel Centre for Advanced Solidification Technology (BCAST), Brunel University London, Uxbridge UB8 3PH, UK; zhichao.niu@brunel.ac.uk (Z.N.); jayesh.patel@brunel.ac.uk (J.B.P.); zhongyun.fan@brunel.ac.uk (Z.F.)

* Correspondence: zhongping.que@brunel.ac.uk; Tel.: +44-1895-268535

Abstract: In addition to impurities in recycled aluminum alloys, non-metallic inclusions are a significant factor that deteriorates the material's castability and final mechanical properties. This, therefore, restricts the ability to transition from a primary to secondary aluminum alloy. In this study, the cleanliness of the recycled A357 alloy was evaluated through non-metallic inclusions' characterization, hydrogen content measurement, fluidity test, and casting defects identification. The non-metallic inclusions generated during the recycling process of A357 alloy were collected by the pressurized melt filtration technique. All of the inclusion types collected during filtration were examined and identified by analytical scanning electron microscopy (SEM). Extra additions of up to 2 wt.% swarf in these secondary A357 alloys were designed to simulate highly contaminated alloys. Different to the conventional melt cleaning technologies that mainly focus on complete removal of inclusions, this study developed a novel approach that combines the removal of easily removeable inclusions while preserving well-dispersed inclusions that do not adversely affect the mechanical properties. This study demonstrates that high shear melt conditioning (HSMC) technology can achieve well-dispersed small non-metallic inclusions, low hydrogen content, improved fluidity, and fewer casting defects. As a result, the melt quality of the recycled A357 alloys has achieved a quality comparable to that of primary A357 alloy.



Citation: Niu, Z.; Que, Z.; Patel, J.B.; Fan, Z. Assessment and Improvement of Melt Quality of Recycled Secondary A357 Alloy by Application of the High Shear Melt Conditioning (HSMC) Technology. *Crystals* **2024**, *14*, 1044. <https://doi.org/10.3390/cryst14121044>

Academic Editor: Benilde F. O. Costa

Received: 27 October 2024

Revised: 20 November 2024

Accepted: 25 November 2024

Published: 30 November 2024



Copyright: © 2024 by the authors. Licensee MDPI, Basel, Switzerland. This article is an open access article distributed under the terms and conditions of the Creative Commons Attribution (CC BY) license (<https://creativecommons.org/licenses/by/4.0/>).

Keywords: recycled A357 alloy; non-metallic inclusions; high shear melt conditioning (HSMC); material castability; mechanical properties

1. Introduction

Aluminum alloys are extensively used in transportation industries because of their advantageous properties of high specific strength, light weight, corrosion resistance, recyclability, and formability, which give them potential in net zero strategies [1]. However, the production of aluminum alloys implies the emission of a high amount of CO₂, which does not align with the sustainability goals of today and the future. On the other hand, as usage increases, issues such as insufficient production of primary aluminum alloy and the accumulation of waste alloys will gradually emerge [2]. Moreover, re-melting of aluminum scrap only requires 5% of the energy needed to produce primary aluminum, and the energy consumed by recycling aluminum is also less than required for primary production; this significantly conserves raw materials such as carbon and alumina [3]. Thus, responsible recycling and reutilization of material in every sector, such as waste electronic devices, scrapped cars, retired aircraft, and discarded construction equipment, are important for economic and environmental purposes to achieve fundamental sustainability [4].

The challenges in recycling aluminum alloys mainly include impurities and non-metallic inclusions (NMIs). Impurity is one of the biggest issues, particularly for wrought aluminum alloys, which have smaller composition specifications. The major concern with

using secondary Al alloys is the tolerance levels for the various elements that can be present without significantly deteriorating the casting performance [5,6]. The list of problematic impurities is quite long, including but not limited to Si, Mg, Ni, Zn, Pb, Cr, Fe, Cu, V, and Mn [7,8]. By far, the most common method to reduce the contents of impurities, such as iron, silicon, and copper, is to add primary aluminum or aluminum alloy into re-melted recycled alloys [9]. However, the high carbon footprint and costs associated with traditional recycling processes remain significant challenges.

NMIs are the second biggest challenge in recycling aluminum alloys. They originate from various sources, including oxidation, excessive addition of grain refiners, alloying, and impurities in aluminum scrap. Al_2O_3 , MgO , MgAl_2O_4 , SiO_2 , FeO , Fe_2O_3 , carbides, such as Al_4C_3 and graphite carbon, and various halides are typical NMIs closely associated with casting defects, such as porosity, hot tearing, and cracking. During the melting process, NMIs can accumulate and adversely affect the overall quality of the recycled alloy. The presence of NMIs can lead to casting defects and compromised performances by the secondary aluminum alloys, including reduced strength, fluidity, ductility, machinability, and corrosion resistance [10]. This restricts the ability to transition from primary to secondary aluminum alloys. Thus, addressing the abovementioned challenges is crucial for improving the reliability of the recycled aluminum alloys.

The current predominant recycling process begins with the sorting of aluminum scrap for re-melting to produce secondary ingots. The alloy's composition is then carefully controlled to meet standardized grades, followed by thorough cleaning and purification to achieve the desired alloy composition for subsequent processing or fabrication [11]. It is well known that the inevitable oxidation of aluminum and its alloys during casting introduces oxide defects that deteriorate the integrity and mechanical properties of the ingots [12,13]. The filming nature of the oxides leads to the formation of re-entrapped bifilms that act as metallurgical defects detrimental to the casting performance [10]. Cleaning the harmful oxides before casting has been one of the most critical procedures in the aluminum foundry industry over the past few decades. In general, detrimental oxides can be partially removed through conventional melt treatments prior to solidification, such as fluxing, degassing (flotation), sedimentation, and filtering [10,14]. Most existing technologies were developed with a focus on complete removal. Therefore, time and efficiency have become the biggest challenges for these conventional methods. This study aims to develop a novel approach that does not remove all inclusions but converts them into a highly dispersed state to minimize their detrimental effects.

High shear melt conditioning (HSMC) is a technology patented by BCAST, Brunel University of London [15]. This technology has been proven in its R&D stage to have significant results with multiple benefits in reducing hydrogen content, reducing the density index (DI), refining the grain size, reducing the number of casting defects, and improving the mechanical properties without the addition of chemical grain refiners or alloying elements [15–17]. In this study, HSMC was employed to address the challenges in aluminum recycling.

2. Experimental

2.1. Materials Preparation and Experimental Setup

In this work, 100% recycled A357 ingots, supplied by commercial manufacturers, were used as raw materials for characterizing non-metallic inclusions. The recycled A357 alloy in this research was purely from post-production materials, such as the cutoff from castings of products not going to market. For each experiment, 10 kg recycled A357 ingots were melted in clay-graphite crucibles using the electric resistance furnace and held for approximately 2 h at 750 °C for homogenization with sufficient stirring. The conventional melt treatment applied in this study is degassing treatment by using a rotary degassing impeller at a speed of 350 rpm for 10 min by injecting pure argon gas at 8 L per minute. Then, 0.15 wt% of Al-5Ti-1B grain refiner and 0.2 wt% of Al-10 wt% Sr master alloy was added to the melt for grain refinement and eutectic Si modification purposes. During the degassing, the melt was covered by a commercial granular flux (FOSECO Coveral GR 2410, Tamworth, England).

The achieve high shear melt conditioning (HSMC) technology was applied to compared with the conventional melt treatment by conducting the intensive melt shearing using a rotor-stator high-shear device prior to casting. During the HSMC, the rotor rotation speed was fixed at 3000 rpm for a predetermined period of time after immersing in the melt. This technique provided both dispersive mixing at the rotor/stator gap and distributive mixing of the dispersed particles in the melt.

After the melt treatment, the recycled A357 melt was poured into a standard mushroom sample ($\varnothing 60 \times 10$ mm) for chemical composition analysis and verification by optical emission spectroscopy (OES). A 3 mm thick as-cast plate was achieved from the mushroom sample which casted in a steel mold, followed by the gridding on 400-grit sandpaper for OES test. The chemical compositions of the primary and recycled A357 alloys were determined and are summarized in Table 1. The reference alloy, A(ref), represents the primary A357 alloy after conventional melt treatment. The Alloy A0 represents the recycled A357 alloy without melt treatment, whereas A1 is the recycled A357 alloy with conventional melt treatment. Alloy A2 includes 2% swarf added after the conventional melt treatment, and alloys A3 and A4 are the same set of materials processed with the HSMC and conventional melt treatments.

Table 1. Elemental compositions of the recycled A357 alloys (wt%).

Alloys	Cu	Mg	Si	Fe	Mn	Ni	Zn	Pb	Sn	Ti	Sr	Be	Al
A(ref)	0.004	0.67	6.54	0.02	0.000	0.000	0.000	0.000	0.000	0.102	0.020	0.000	Bal.
A0	0.008	0.68	6.59	0.05	0.005	0.002	0.004	0.000	0.003	0.148	0.012	0.000	Bal.
A1	0.007	0.64	6.60	0.05	0.004	0.003	0.004	0.000	0.003	0.138	0.014	0.000	Bal.
A2	0.007	0.67	6.62	0.05	0.004	0.003	0.004	0.000	0.003	0.138	0.017	0.000	Bal.
A3	0.007	0.63	6.56	0.05	0.004	0.002	0.004	0.000	0.003	0.140	0.022	0.000	Bal.
A4	0.007	0.65	6.63	0.05	0.004	0.002	0.004	0.000	0.003	0.138	0.019	0.000	Bal.

A pressurized melt filtration technique was utilized to collect and facilitate the direct examination of the inclusions in the recycled A357 melts. A total of 2 kg from each 10 kg melt in each trial was transferred to a preheated filtration crucible equipped with a ceramic filter with an average pore size of 90 μm at the bottom of the unit. Argon gas was introduced at a pressure of 4 PSI to force the liquid melt through the filter and isolate the melt from air. As a result, the inclusions gradually accumulated above the filter.

2.2. Characterization of Non-Metallic Inclusions

To determine the characteristics of the concentrated NMIs, filtration samples were sectioned perpendicular to the filter. The NMIs collected in each sample were then examined using a Carl Zeiss Crossbeam 340 scanning electron microscope (SEM) equipped with an energy-dispersive X-ray spectrometer (EDS). To quantify the sizes and size distribution of the inclusion particles, comparable images of the same area of inclusions were selected for each set of melt conditions. The sampling was conducted by counting and measuring the size of each individual particle or film in the same imaging area to ensure the accuracy for comparison. The sizes of the inclusion particles were measured directly from SEM images using the image-processing software Fiji Image J.

2.3. Material Properties and Melt Quality Characterization

The hydrogen concentrations in the melts were measured directly using a FOSECO ALSPEK-H probe. The probe was immersed at a depth of between 150 and 200 mm inside the melt. The readings were given in units of mL/100 g with real-time data. A reduced pressure test (RPT) was also conducted to measure the density index (DI) value, which roughly represents the gas content and inclusion levels. This method involves solidifying the melt into two conical steel cups, one in air (atmospheric pressure) and the other under

partial vacuum (80 mbar). With the intention of testing the fluidity of the recycled alloys, the melt was poured at 720 °C into an ASTM standard spiral flow fluidity test mold, which was preheated at 400 °C. Three fluidity tests and three density tests were conducted for each melt condition to provide accurate average values of spiral flow length and porosity percentage, respectively. A standard K-mold for the fracture test was used to check for macro defects. Liquid metal was cast into a mold featuring notches. Once solidified, the resulting bar was bent to expose a fractured surface. Five samples were cast for each melt condition. A visual observation of the inclusions on the fracture was used to determine a K-value for the melt quality and compared to a pre-set standard. However, this method is rather imprecise and, therefore, only suitable for detecting large inclusions and inclusion clusters.

3. Results

3.1. Identification of the Predominant Inclusions in the Primary A357 Alloys

To compare the cleanliness of the melts between the primary and recycled A357 alloys, the inclusions in the primary A357 alloy after melt filtration were firstly characterized as the reference. After conventional melt treatment, the number density of the inclusions was small, as shown in Figure 1a. According to the SEM-EDS analysis, the inclusions collected from the melt were identified as mainly native oxides, which existed as either individual particles or continuous films. The TiB_2 particles, which were added in the form of grain refiner during the melt treatment, were identified as the other inclusions in the filtration sample (Figure 1b). These particles were well distributed in the melt, with the size of one hundred nanometers. Another type of inclusion found in the melt was primarily young oxide bi-films [18], which mainly consisted of individual $MgAl_2O_4$ particles within the Al matrix (Figure 1c,d).

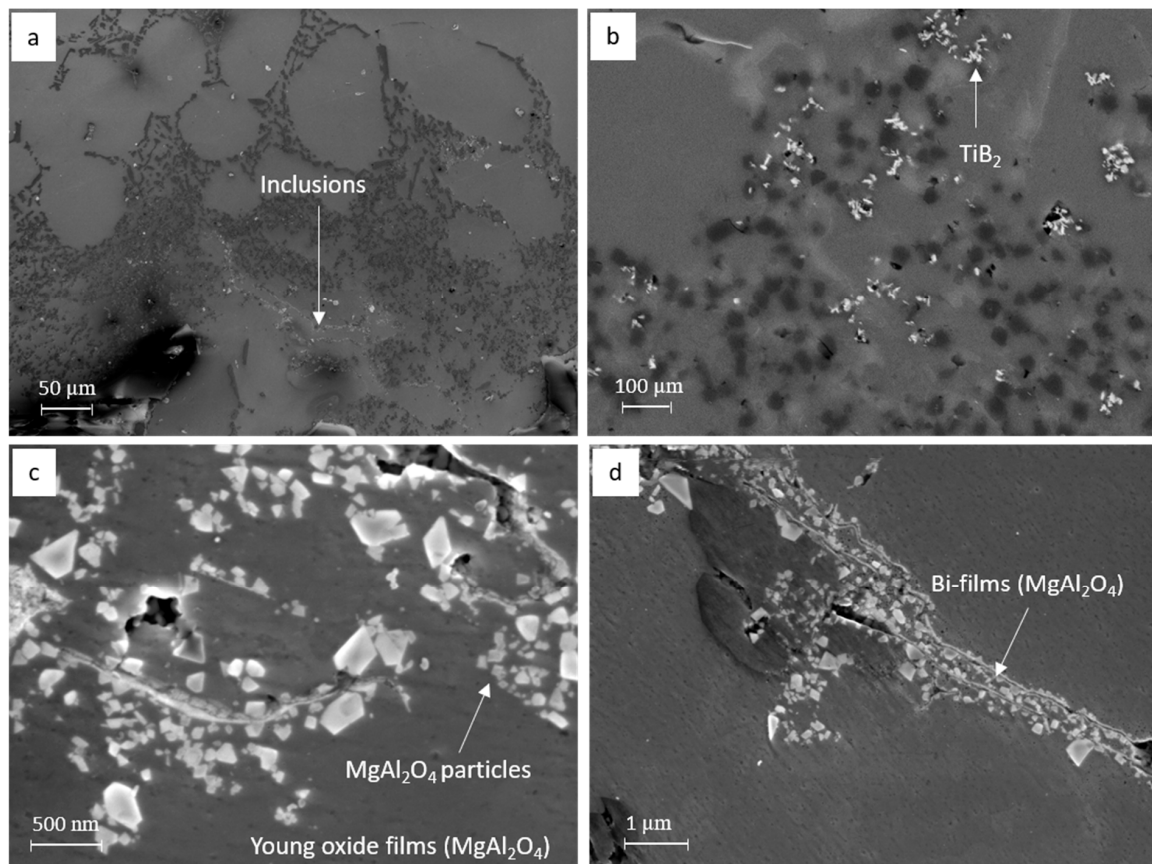


Figure 1. Identification of the inclusions in the filtrated sample of primary A357 alloy after conventional melt treatment for the A(ref.): (a) inclusion band; (b) TiB_2 particles; (c) young oxide films ($MgAl_2O_4$); (d) oxide bi-films ($MgAl_2O_4$).

3.2. Identification of the Predominant Inclusions in the Recycled A357 Alloys

Contrary to the primary A357 melt, the inclusions observed in the previously recycled melts were hardly removed by the conventional melt treatment. As shown in Figure 2, the inclusions filtered from the recycled A357 alloys had a dramatically large number density, with a more than 1500 μm inclusion band width. Additionally, the inclusions were often found in the continuous form, which can lead to large defects that are extremely detrimental to the properties of the cast samples.

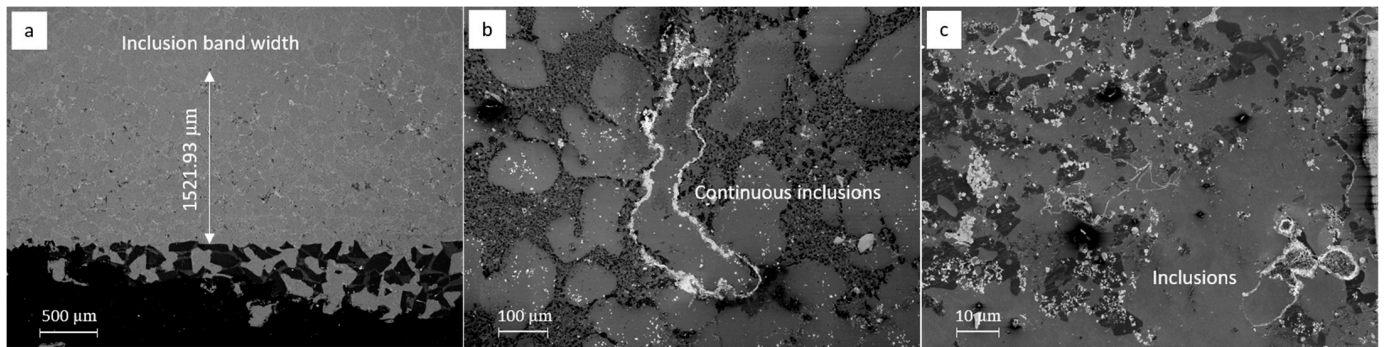


Figure 2. Inclusions in the recycled A357 alloys (A0) collected with the pressurized melt filtration showing: (a) the wide inclusion band; (b) inclusions in the continuous form; (c) inclusions with a large number density.

Oxide films, which are composed of discrete oxide particles on the nanometer scale, were the major constituents of inclusions found in the recycled A357 alloys. As shown in Figure 2b,c, both young and old films were extensively collected in the filtered samples. The young films were flexible liquid films, identified as oxidation on the freshly exposed melt surface for a short period of time during the melt's preparation and handling. A representative young oxide film in the recycled A357 alloy is shown in the SEM image (Figure 3a). Detailed observations reveal that this film is in the discontinuous form and composed of MgAl_2O_4 particles with a broad size range, as detected by the SEM-EDS. Among these, the octahedron can be recognized as the common two-dimensional (2D) morphology for the constituent MgAl_2O_4 particles. A typical old film, measuring a few microns in thickness and extending up to hundreds of microns in length, is identified as MgAl_2O_4 , as shown in Figure 3b. The old oxide film is found to be relatively stiff as a result of the long-term oxidation of the melt surface compared to the young films. The coarse oxide particles form a relatively dense skull on one surface, which can easily develop into continuous films that undergo oxidation due to the supply of oxygen during recycling. Moreover, bi-films, which are increasingly recognized as a source of metallurgical defects, were also extensively found in the recycled A357 alloys. These films are known to fold over and submerge in the bulk liquid with a volume of air entrapped within it. Either Al_2O_3 or MgAl_2O_4 particles were identified via SEM-EDS on each side of the film, as shown in Figure 3c. In addition, discontinuous young oxide films consisting of Al_2O_3 particles exhibiting the morphology of platelets were also found, as shown in Figure 3d. However, the number density was relatively small compared to that of MgAl_2O_4 .

In addition to the major oxide inclusions, nitride inclusions and carbide inclusions, which are rarely found in primary aluminum alloys, were extensively observed in the recycled A357 alloys. However, the number density was still relatively small compared to that of the oxides. Figure 4a,b show micrographs of the typical nitride and carbide particles detected in the filtrated sample. Most of the aluminum nitride inclusion particles exhibited short rod-like morphologies in 2D cross-sections, detected as AlN by SEM-EDS. Aluminum carbide inclusion particles were detected as Al_4C_3 in the filtration sample. These carbide inclusion particles exhibited hexagonal or grey disc morphologies, and typically were found as isolated clusters or with oxide and boride particles.

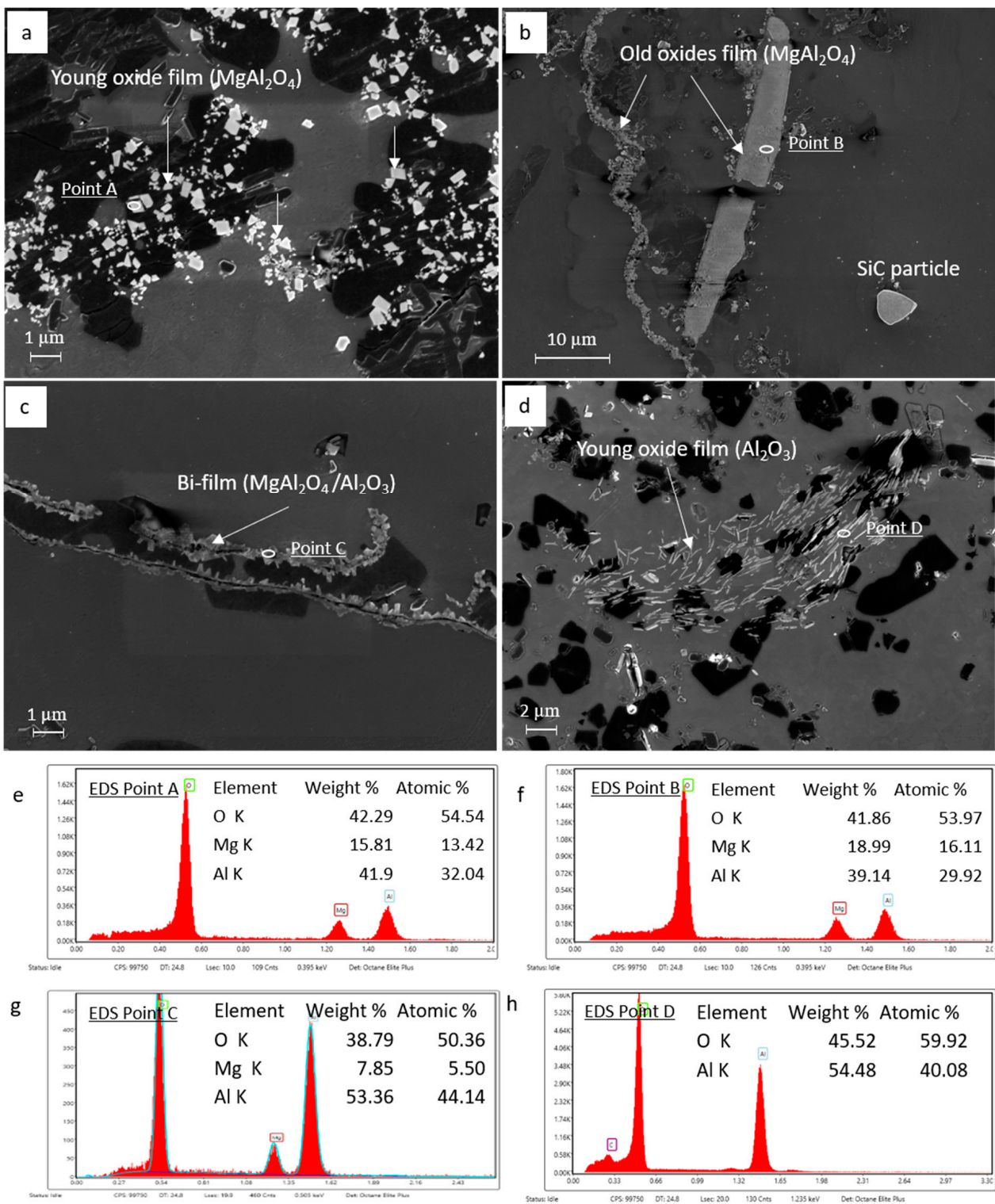


Figure 3. Identification of inclusions in the filtration sample of the recycled A357 alloy (A0): (a) young oxide films (MgAl_2O_4); (b) old oxide films (MgAl_2O_4); (c) bi-films ($\text{MgAl}_2\text{O}_4/\text{Al}_2\text{O}_3$); (d) young oxide films (Al_2O_3); (e–h) chemical compositions of the identified inclusions.

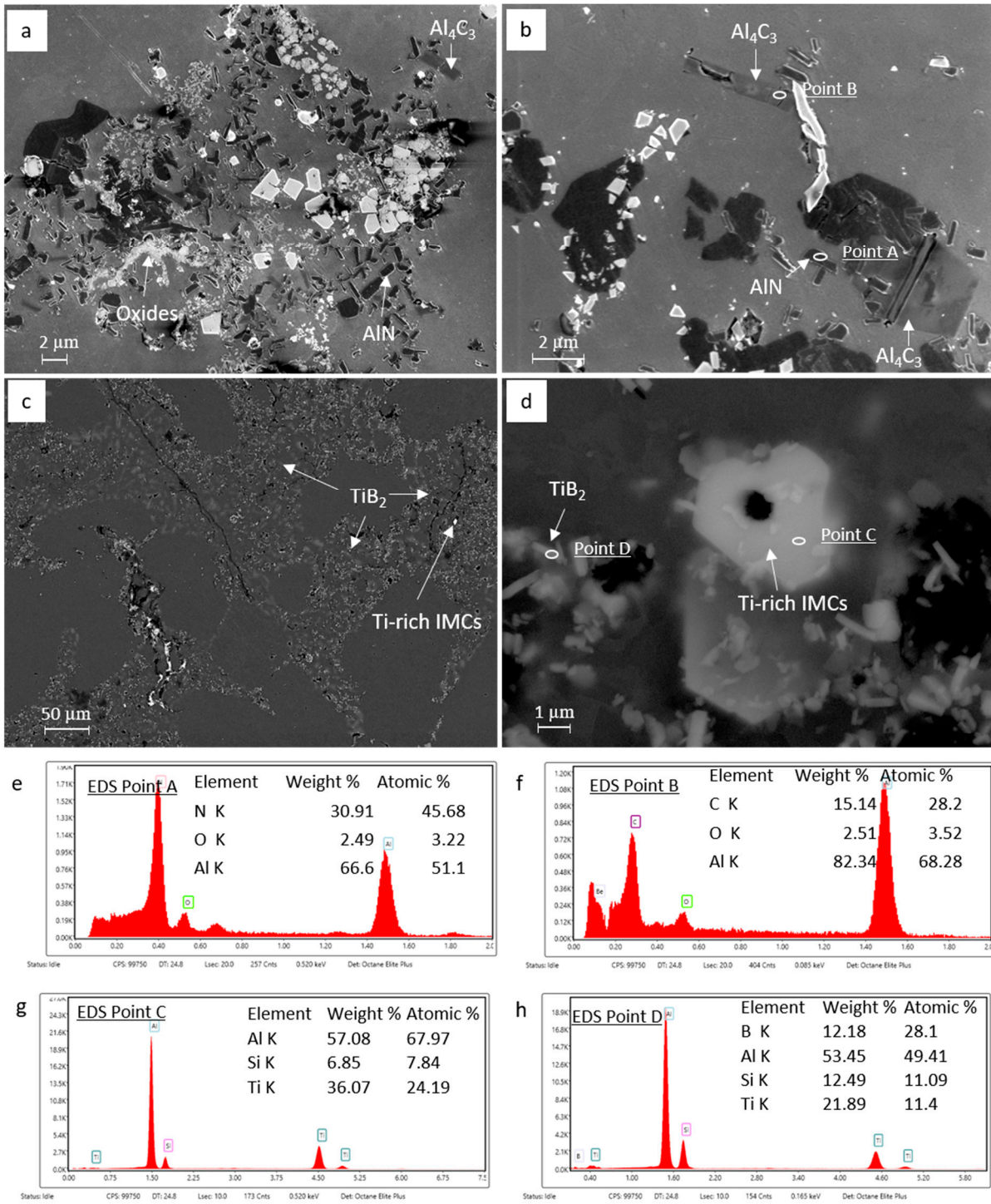


Figure 4. The collected inclusions in the filtration sample from the recycled A357 alloy (A0) showing (a) the inclusions mainly contain $MgAl_2O_4$, AlN and Al_4C_3 , and TiB_2 ; (b) the morphology of AlN and Al_4C_3 particles; (c) TiB_2 ; (d) a few primary Ti -rich IMCs; (e–h) chemical compositions of the identified inclusions.

TiB₂ particles, with an extremely large number density, as shown in Figure 4c, represent another major inclusion type identified in the recycled A357 alloys. These TiB₂ particles were extensively found at the grain boundary in the filtration samples. Large Ti-rich intermetallic compounds (IMCs) with sizes ranging from a few tens of microns to one hundred microns were also observed in the recycled A357 alloys. These coarser Ti-rich IMCs, typically nucleated by an oxide inclusion containing various impure elements, as shown in Figure 4d, can easily cause fractures and are detrimental to the mechanical properties. However, the number density of these IMCs was extremely small compared to that of other inclusions. Thus, they were not considered an important factor in the deterioration of the mechanical properties of the recycled A357 alloys.

3.3. Characterization of Inclusions in the Recycled A357 Alloys under Different Melt Conditions

Characterization of the inclusions in the recycled A357 alloys under different melt conditions was conducted on the filtration samples, as shown in Figures 5–9. The results in Figure 5 show that the inclusion band width of the recycled A357 alloy was 636.84 μm, while it increased to 1267.43 μm after the addition of 2% swarf. However, after the HSMC, the values dropped to 343.80 μm and 514.55 μm for the non-addition sample and 2% swarf addition, respectively. This indicates that the total number of inclusions increased after the addition of 2% swarf, while it significantly decreased after the HSMC. Further examinations of the types and morphologies of the inclusions were conducted for each condition. For the recycled A357 alloy after the conventional melt treatment, the inclusions mainly consisted of agglomerated oxide films/particles and TiB₂ particles, as shown in Figure 6. It can also be seen that AlN and Al₄C₃ particles were still present, especially within the oxide films, along with a small number of IMCs, such as Ti-rich IMCs and Fe-rich IMCs. Similar to the recycled A357 alloy, the inclusions in the melt with the 2% swarf addition mainly consisted of oxides and TiB₂, along with a few nitrides, carbides, and IMCs. Moreover, the young films consisted of individual oxide particles, and more nitride and carbide particles were significantly observed after the swarf additions, as shown in Figure 7. This is due to the re-melting of the swarf, which introduces more fresh oxides from the melt surface. Additionally, the burning of the swarf results in chemical reactions that form nitride and carbide particles, which become entrapped in the melt as harmful inclusions.

In terms of the effects of the HSMC, the SEM micrographs show that the inclusion particles become more discrete, with significant reductions in size and number density. The TiB₂ particles, which were concentrated in the grain boundaries, have been de-agglomerated with a much better distribution. The old inclusion films were rarely observed, and inclusion particles in the form of continuous films were significantly reduced after the HSMC. This is attributed to the intensive melt shearing effectively breaking up the entrapped inclusions and films, which remain as existing inclusions but in a highly dispersed state. This enables the possibility of more inclusions being removed during the following degassing treatment. On the other hand, even the inclusions that were collected during the filtration may gather again, and the morphologies of the identified inclusions, as shown in Figures 8 and 9, still demonstrated that the HSMC further promotes the dispersity of the inclusions. However, the types of inclusions in the recycled A357 alloys had no differences before (Figures 6 and 7) and after the HSMC (Figures 8 and 9).

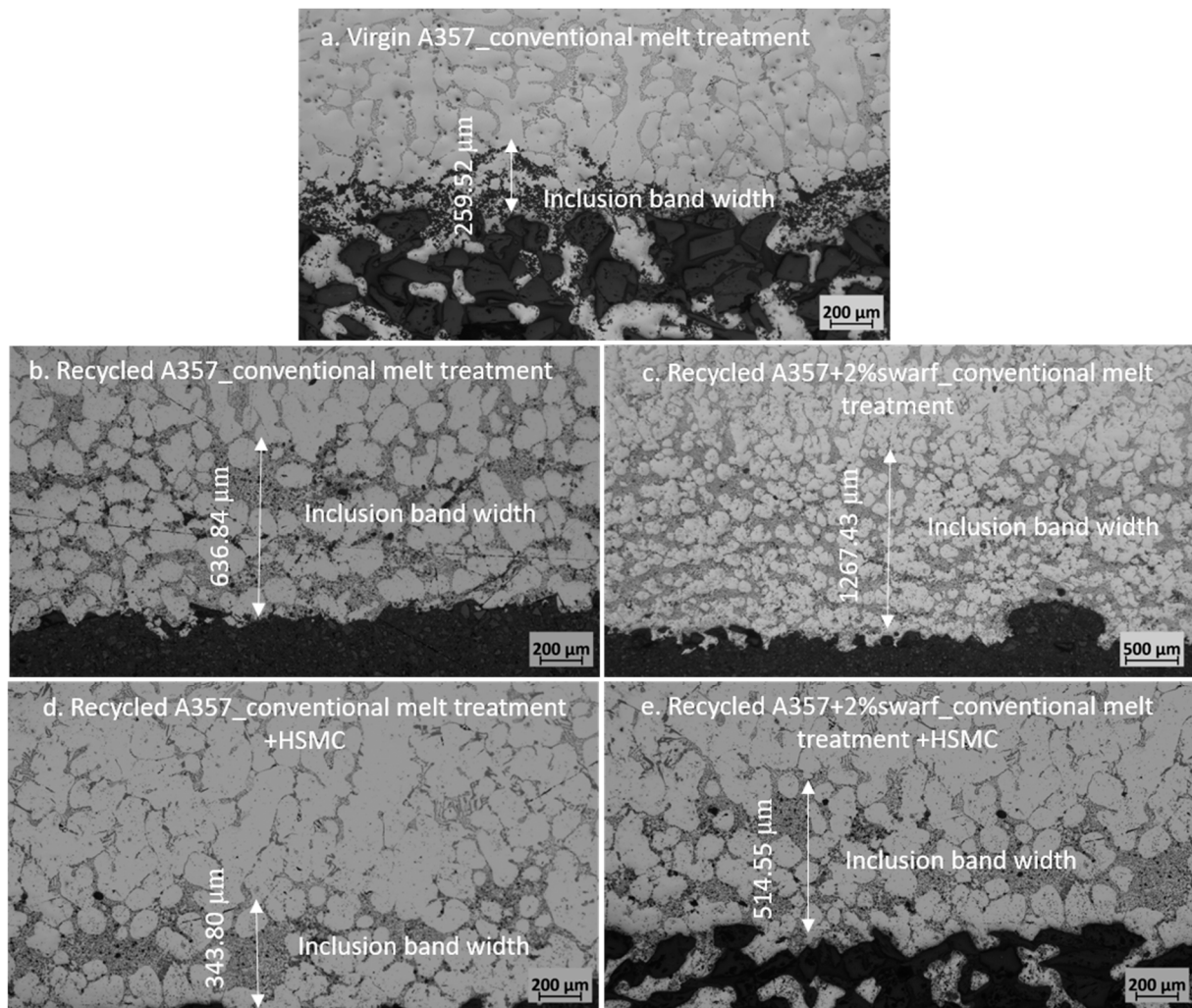


Figure 5. SEM micrographs showing the inclusion band width as a reflection of the number density of the inclusions in the recycled A357 alloy under different melt conditions: (a) primary A357 after conventional melt treatment (A(ref)); (b) recycled A357 after conventional melt treatment (A1); (c) recycled A357+2% swarf after conventional melt treatment (A2); (d) recycled A357 after conventional melt treatment and HSMC (A3); (e) recycled A357+2% swarf after conventional melt treatment and HSMC (A4).

3.4. Variations in the Size and Number Density of Inclusions in the Recycled A357 Alloys

To quantify the sizes of the inclusions, particles of each identified inclusion under different melt conditions were measured individually. The results provided in Table 2 show the average sizes of the inclusion particles in the recycled A357 alloys, as well as the differences in the geometric mean diameter and standard deviation. As can be observed from the results, TiB_2 , as one of the most dominant inclusions in the recycled A357 alloys, had similar mean sizes and standard deviations under all melt conditions. Without the HSMC (A1 and A2), the mean sizes of the AlN particles were measured to be 867 nm and 771 nm in the recycled A357 alloy and recycled A357 alloy plus 2% swarf addition, respectively, which are both slightly larger than that of the AlN particles, which were 879 nm and 765 nm in both alloys after applying the HSMC (A3 and A4). This suggests that the addition of swarf introduced fresher AlN particles with smaller sizes, which were sufficient in quantity to influence the mean sizes of the AlN particles in the melt. In addition, the dispersion by HSMC had no effects on the size and size distribution of the AlN particles. Similar to the results for the nitride particles, the swarf addition had the same effects on the Al_4C_3 particles found in the melts. The sizes of the Al_4C_3 particles

slightly decreased from 2009 nm and 1927 nm in melts A1 and A3 to 1522 nm and 1579 nm in melts A2 and A4 after the addition of 2% swarf. Marginally, the size and distribution of the oxides were significantly different after the various melt treatments. After adding 2% swarf, it was observed that the geometric mean of the particle sizes of the oxide particles slightly decreased from 580 nm to 481 nm for the non-HSMC samples and from 337 nm to 317 nm for the HSMC samples. This can be attributed to the swarf introducing fresh oxides, primarily in the form of γ - Al_2O_3 , which have small particle sizes and insufficient time to grow in the melt. However, the oxides were still dominated by old MgAl_2O_4 particles with relative larger particle sizes. Moreover, the size of the oxide particles after the HSMC was dramatically smaller (337 nm and 317 nm) than those of the non-HSMC (580 nm and 481 nm) samples. This is due to the dispersive power of HSMC, which eliminated the uneven size distribution by breaking the larger oxide films into smaller individual particles, leading to well-dispersed oxides with a narrow size distribution but smaller particle sizes. The values of the standard deviation for all melts were consistent. Furthermore, the lengths of the oxide films were found to be larger after the swarf addition due to the existence of young, continuous films. The average length increased from 39 μm to 60 μm upon addition of 2% swarf to the recycled A357 melt. However, the dispersity promoted by the HSMC treatment helped to break up the continuous oxide films, allowing them to be well dispersed in the melt. Figures 8 and 9 show that the continuous oxide films disappeared after the HSMC, replaced by the discontinuous pieces with discrete oxide particles.

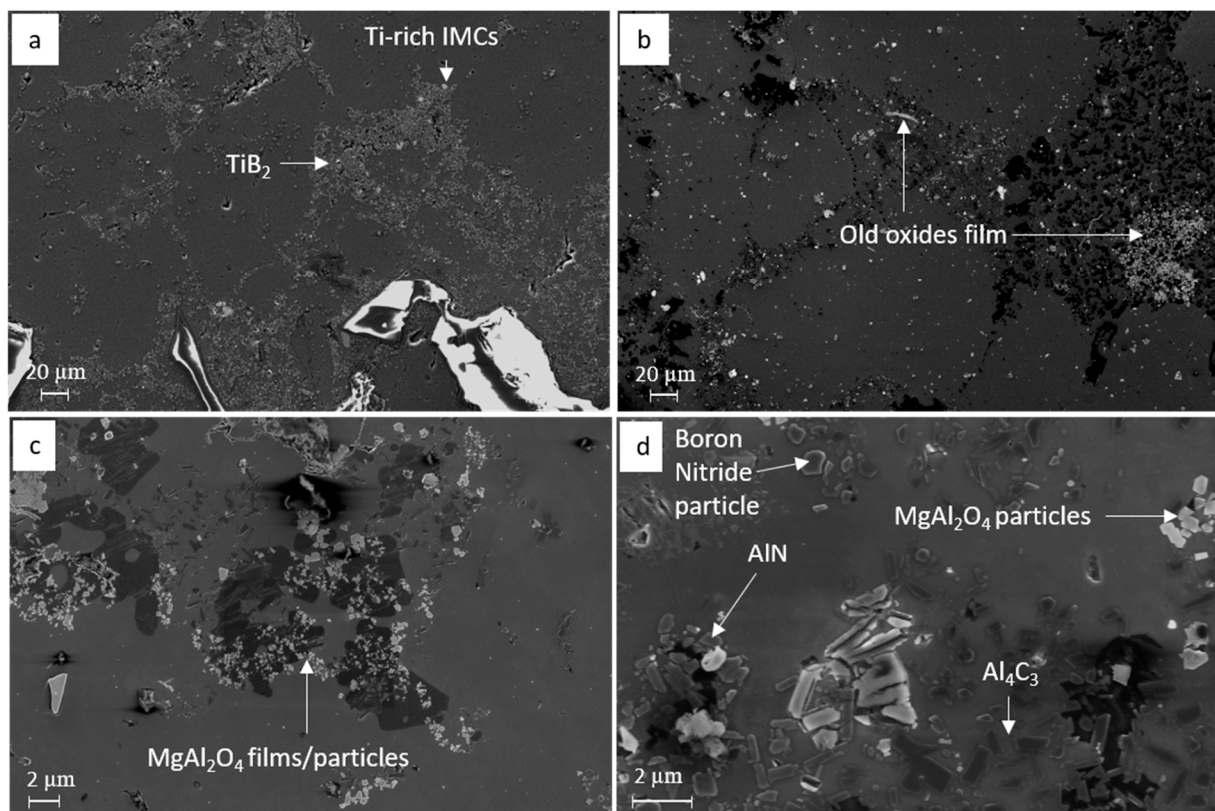


Figure 6. Identification of the inclusions in the filtration sample of the recycled A357 alloy after conventional melt treatment (A1). (a) agglomerated TiB_2 and Ti-rich IMCs with large number density; (b) large old oxide films; (c) MgAl_2O_4 in oxide films; (d) AlN and Al_4C_3 particles with large number density.

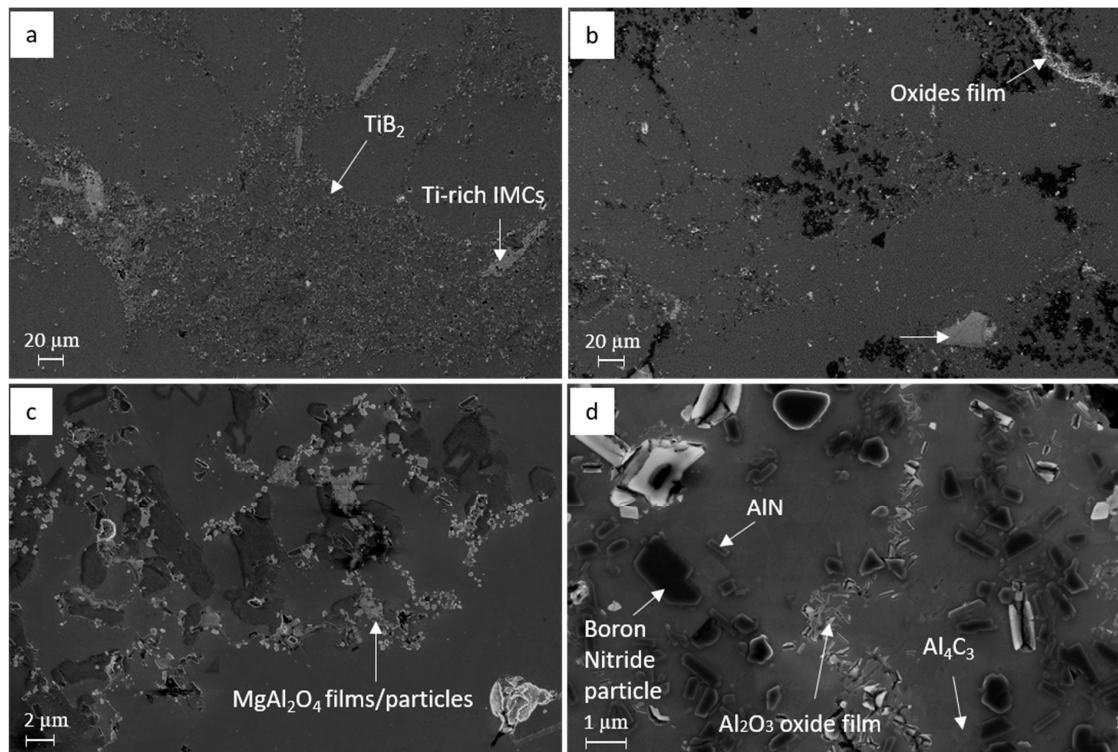


Figure 7. Identification of the inclusions in the filtration sample of the recycled A357 alloy with 2% swarf added after conventional melt treatment (A2). (a) agglomerated TiB_2 and Ti-rich IMCs with large number density; (b) large old oxide films; (c) $MgAl_2O_4$ in oxide films; (d) old and fresh AlN and Al_4C_3 particles with large number density.

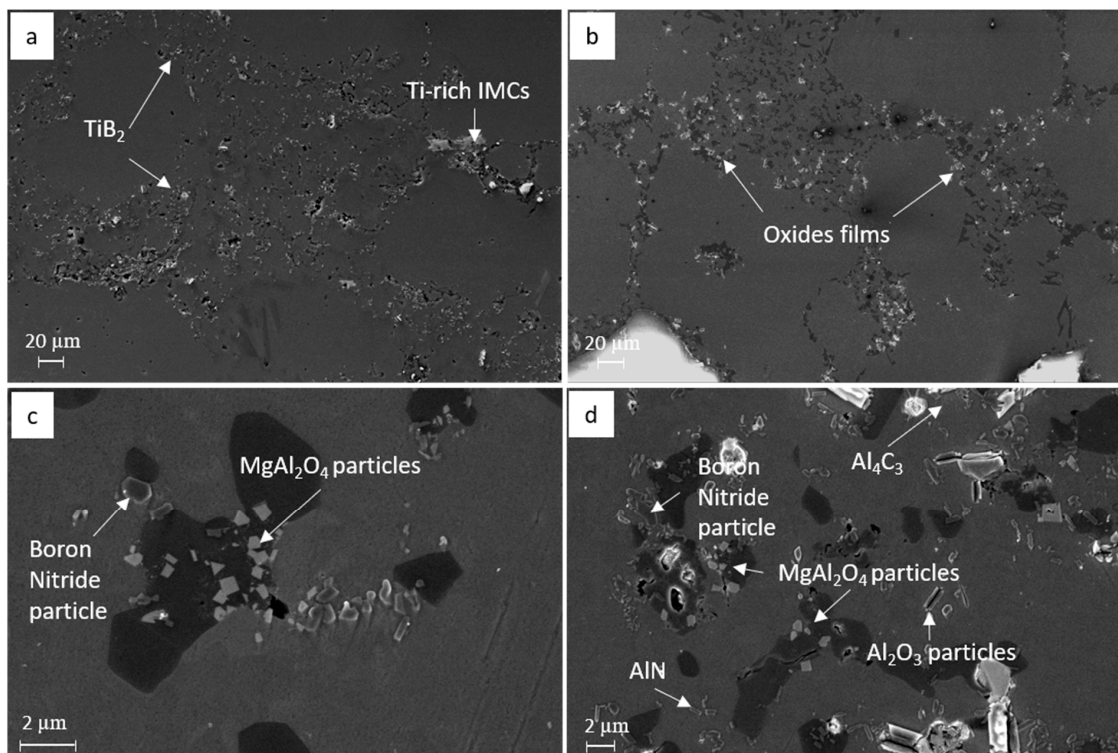


Figure 8. Identification of the inclusions in the filtration sample of the recycled A357 alloy after the HSMC (A3). (a) well dispersed TiB_2 and Ti-rich IMCs with smaller number density; (b) dispersed old oxide films with smaller size; (c) $MgAl_2O_4$ in oxide films; (d) Al_2O_3 , AlN and Al_4C_3 particles.

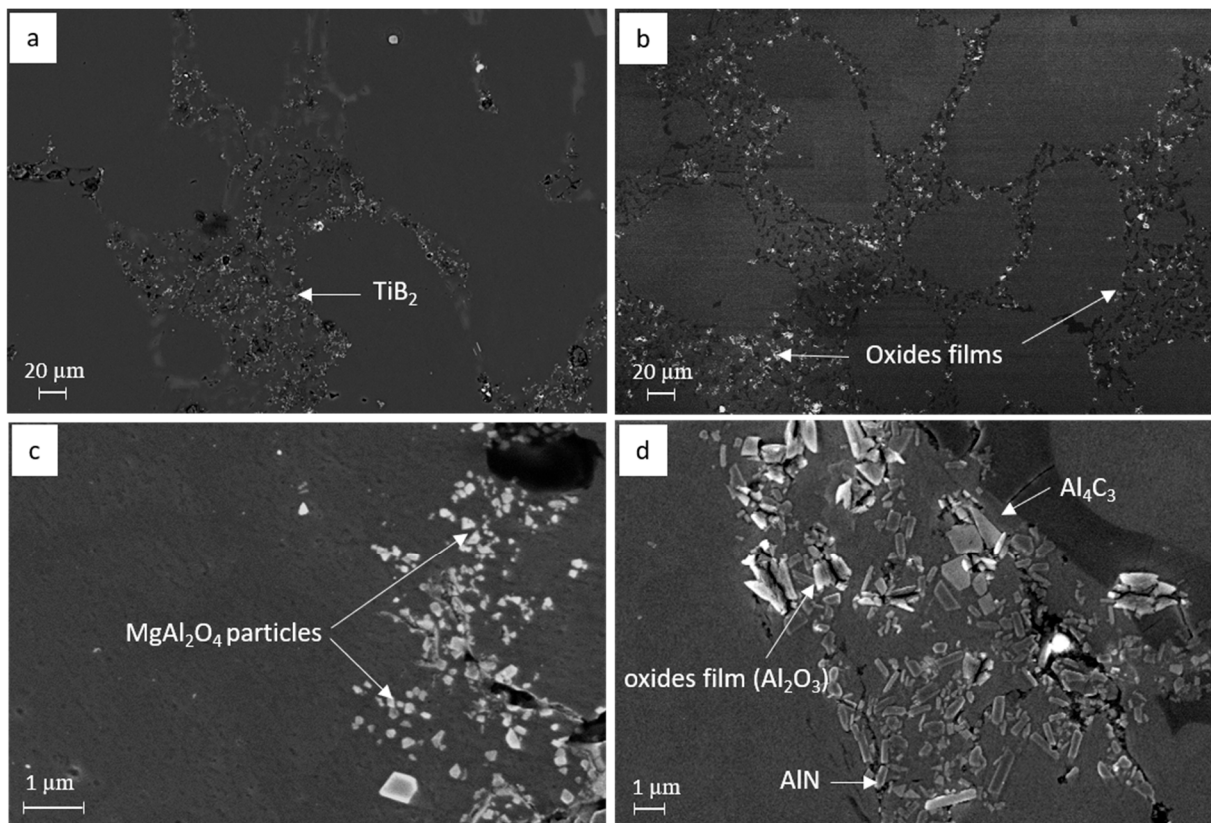


Figure 9. Identification of the inclusions in the filtration sample of the recycled A357 alloy with 2% swarf added after the HSMC (A4). (a) well dispersed TiB_2 and Ti-rich IMCs with smaller number density; (b) dispersed old oxide films with smaller size; (c) $MgAl_2O_4$ in oxide films; (d) old and fresh AlN and Al_4C_3 particles with large number density.

Table 2. Inclusion sizes in the recycled A357 alloys under various melt conditions.

	TiB_2 (nm)	AlN (nm)	Al_4C_3 (nm)	Oxide (nm)	Oxide Film (μm)
A1	986 ± 188	867 ± 223	2009 ± 398	580 ± 163	39 ± 11
A2	949 ± 158	771 ± 202	1522 ± 471	481 ± 134	60 ± 22
A3	987 ± 176	879 ± 213	1927 ± 411	337 ± 121	17 ± 3
A4	949 ± 158	765 ± 177	1579 ± 429	317 ± 101	20 ± 9

In terms of the number density of the inclusions in the recycled A357 alloy, it was difficult to identify the inclusions in the cast sample. On the other hand, the inclusions collected via pressurized filtration were concentrated again, which is also not conducive to an analysis of the number density. Thus, the inclusion band width, as a reflection of the total number of inclusions in the filtration sample, was applied to represent the number density. Figure 5a–e show micrographs of the inclusion band width of the filtration samples for the primary and recycled A357 alloys before/after 2% swarf addition with and without HSMC, respectively. Compared with the inclusion band width of the primary A357 alloy, as shown in Figure 5a, the recycled A357 alloy consistently exhibited a much higher number density of inclusions. The value of the inclusion band width increased after adding 2% swarf, indicating that the swarf addition introduced more fresh inclusions into the melt concentrate and which were retained by the filter. As a result, the number density of the inclusions significantly increased. Compared with the non-HSMC samples, the melts after HSMC had relatively smaller band widths. The HSMC contributed to the dispersity and further removal of the inclusion particles and films, resulting in a reduction in the inclusion number density of both melts with/without additional swarf. As a result, the

combination of the conventional melt cleaning processes with HSMC technology is an effective method for achieving well-dispersed oxide inclusions within a melt, without removing all inclusions but converting them into a highly dispersed state to minimize their detrimental effects, as shown in Figures 8 and 9.

3.5. Effects of Inclusions on the Melt Quality and Material Properties of the Recycled A357 Alloys

To further investigate the effect of the inclusions on the melt quality and material properties, the melt filtration curves, melt hydrogen content and density index, melt fluidity, and the fracture behavior of the recycled A357 alloy were further examined.

The filtration curves of the recycled A357 alloys with/without 2% swarf addition for both the HSMC and non-HSMC samples are shown in Figure 10. As the inclusions in the melt gradually become blocked and accumulated above the filter, the completion of the pressurized filtration was set to either a filtration time of 150 s or a filtration weight of 1.4 kg. The filtration curves show that the total weights of the melts filtered out after 2 wt.% swarf additions were much smaller than those without any addition for both samples with/without HSMC. This indicates that after the conventional melt treatment, the melt with 2% swarf addition had a higher presence of inclusions, which concentrated and blocked the filter in the early stage. Moreover, the total melt filtration weight for the non-HSMC samples was smaller than those with HSMC. This means that HSMC is effective in delaying filter blockage, allowing more melt to pass through the filter. This further confirms the previously mentioned results regarding the total inclusion amount, as shown in Figure 5.

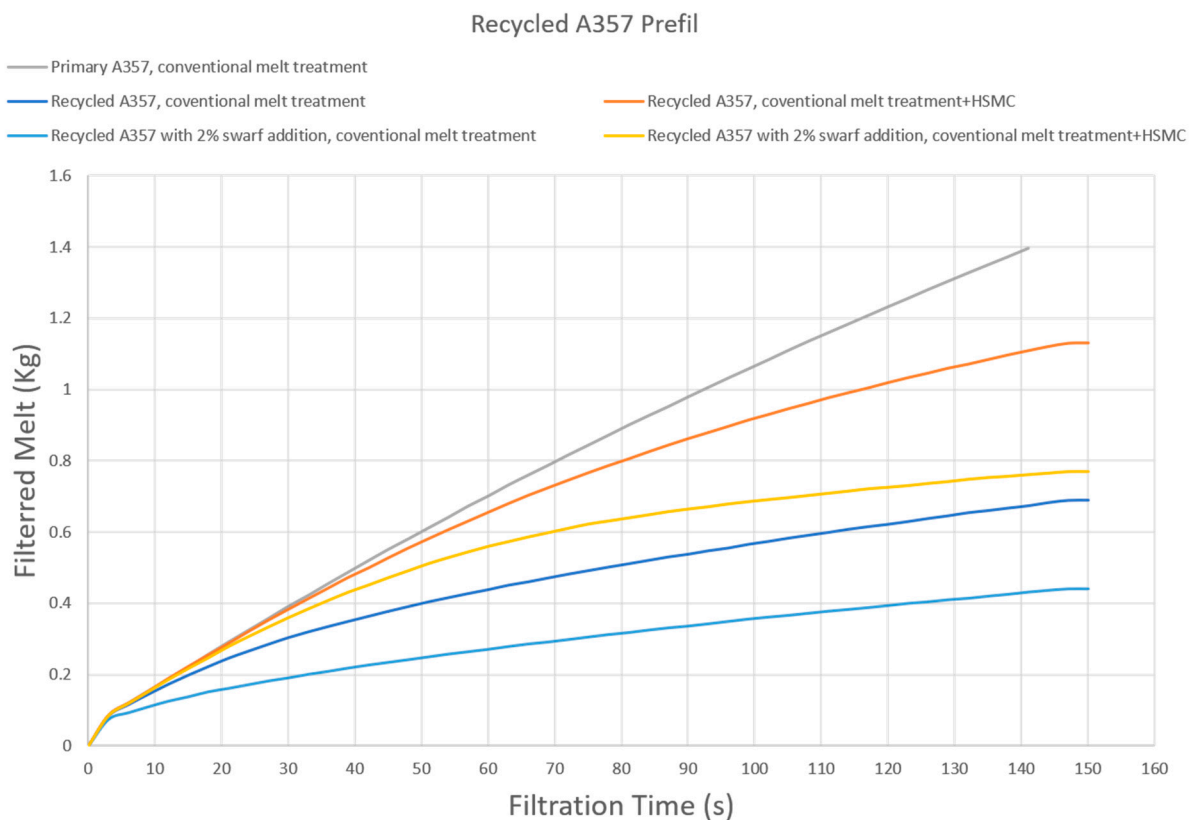
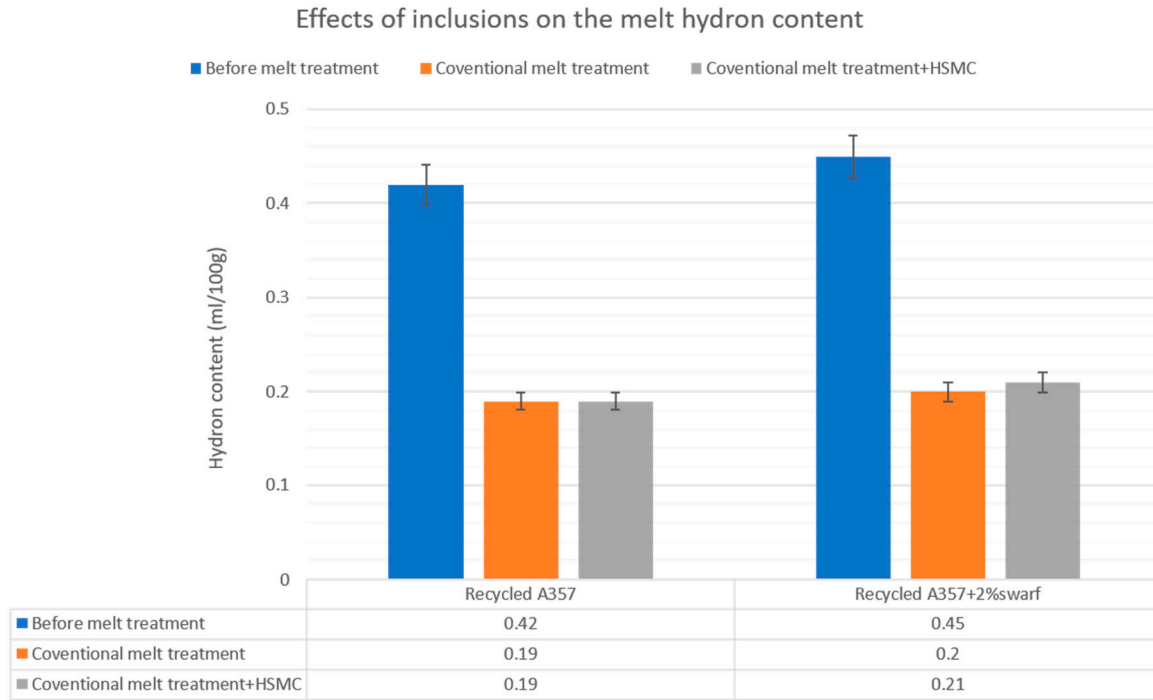


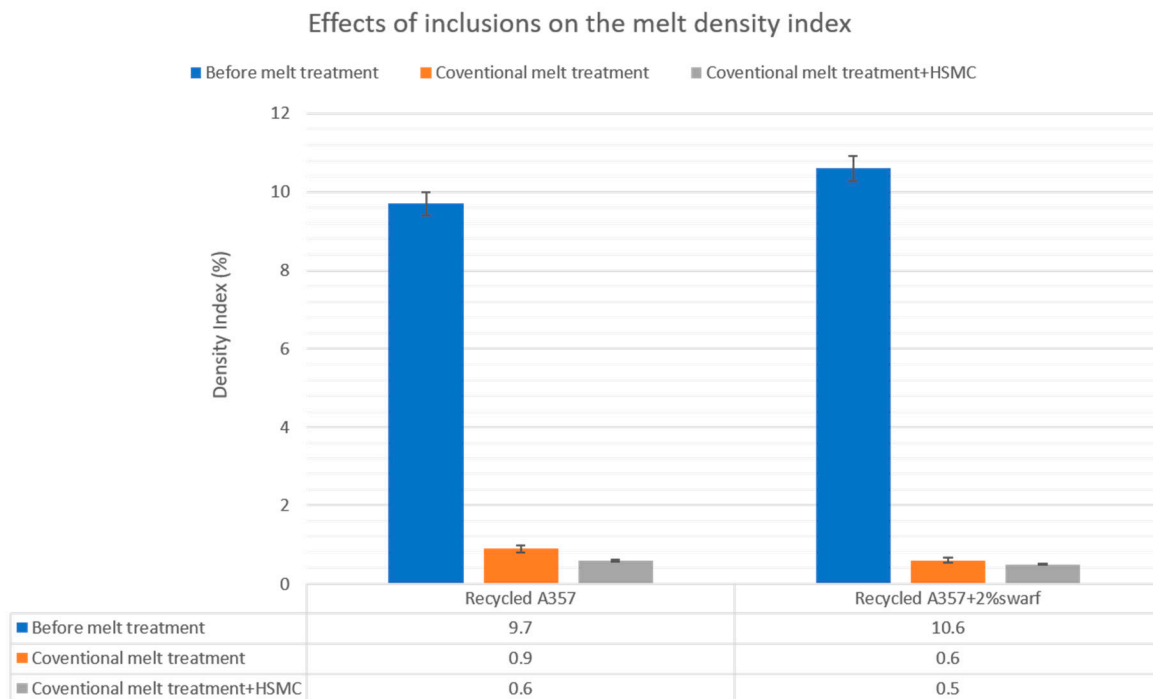
Figure 10. Melt filtration curves of the A357 alloys under different melt conditions.

Figure 11 displays the hydrogen content and density index of the recycled A357 alloy under various melt conditions and treatments. All melts began with a comparable initial hydrogen content, which was relatively high. Both conventional melt treatment and HSMC combined with conventional melt treatment were found effective in removing hydrogen from the melts, whether or not swarf was added, achieving a similar equilibrium value of

0.20 mL/100 g. The results from the density index evaluation also showed no difference for all melt conditions (DI around 0.6%). This confirms that swarf additions will not affect the H content and DI value after the melt treatment. On the other hand, HSMC, as an addition melt treatment process conducted before conventional rotary degassing, did not affect the final hydrogen content and DI value. Therefore, these two values were influenced solely by the conventional degassing process.



(a)



(b)

Figure 11. (a) The effects of inclusions on the melt hydrogen content and (b) density index of the recycled A357 alloy before and after melt treatment.

The effects of the additional swarf and HSMC on the melt fluidity evolution of the recycled A357 alloy are shown in Figure 12. It can be observed that with swarf additions, the melt fluidity decreased from 875 mm to 838 mm, attributed to the significant increase in the amount of inclusions, as illustrated in Section 3.3 (Figures 6–9). HSMC, as an effective method for dispersing existing inclusions and aiding their removal from the melt, contributed to an increase in the melt fluidity, rising from 875 mm to 905 mm for the non-addition condition and from 838 mm to 863 mm for the melt with 2% swarf addition. From the results, HSMC was found to restore the fluidity of the melt with 2% swarf addition to levels similar to those observed previously. This demonstrates the potential to achieve equivalent melt qualities from recycled aluminum alloys comparable to primary aluminum alloys by applying HSMC technology.

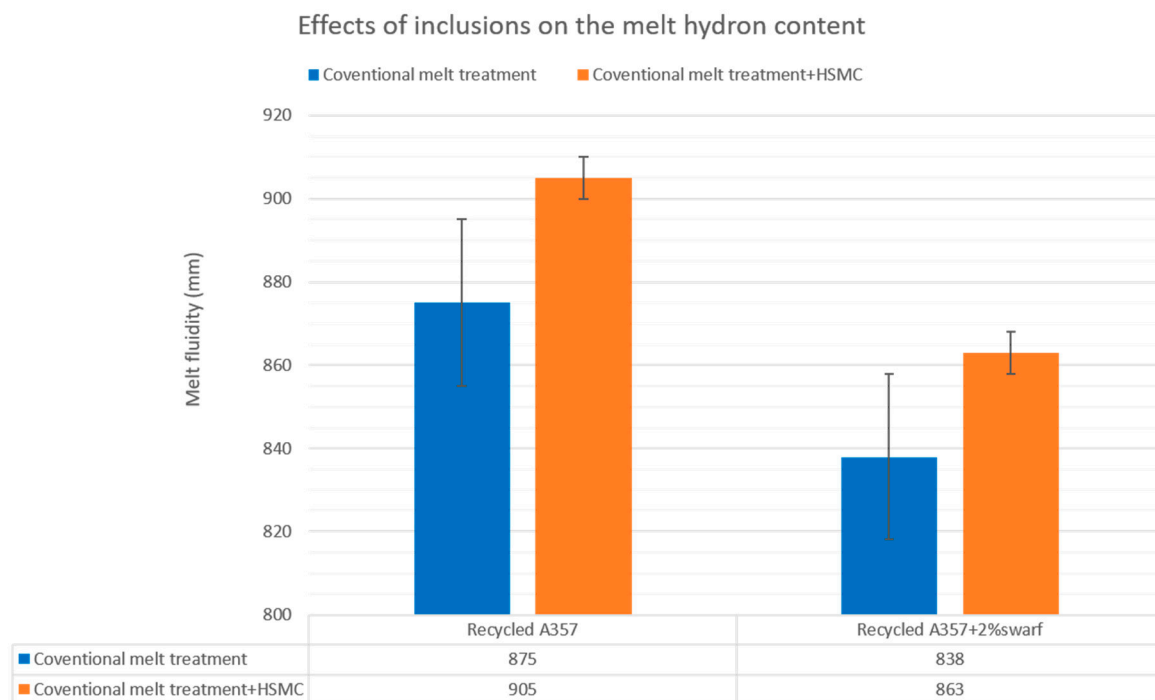


Figure 12. The effects of inclusions on the melt fluidity of the recycled A357 alloy before and after the melt treatment.

The melt cleanliness was further examined and quantified via the K-mold fracture test. Figure 13 shows the size and size distribution of the K-mold fracture defects under different melt treatments. The number density of the defects increased significantly after 2% swarf addition. The average size of the fracture defects was slightly smaller and the size distribution became more uniform due to the extensive amount of freshly formed inclusions with a smaller size in the melt. However, a large number density of total inclusions with poor agglomeration results in a low mechanical property. In terms of the HSMC, its dispersive effects facilitate further inclusion removal and break up residual inclusions. A melt dominated by relatively smaller inclusion particles is then achieved. As a result, both the number density and size of the fracture defects are found to be significantly reduced after HSMC. Additionally, the size distribution of these defects becomes more uniform, as shown in Figure 12, where large defects in the 0.2–0.5 mm range disappear and are replaced by smaller defects. Thus, HSMC has the potential to enhance the castability of the recycled A357 alloy by reducing the size and continuity of the defects.

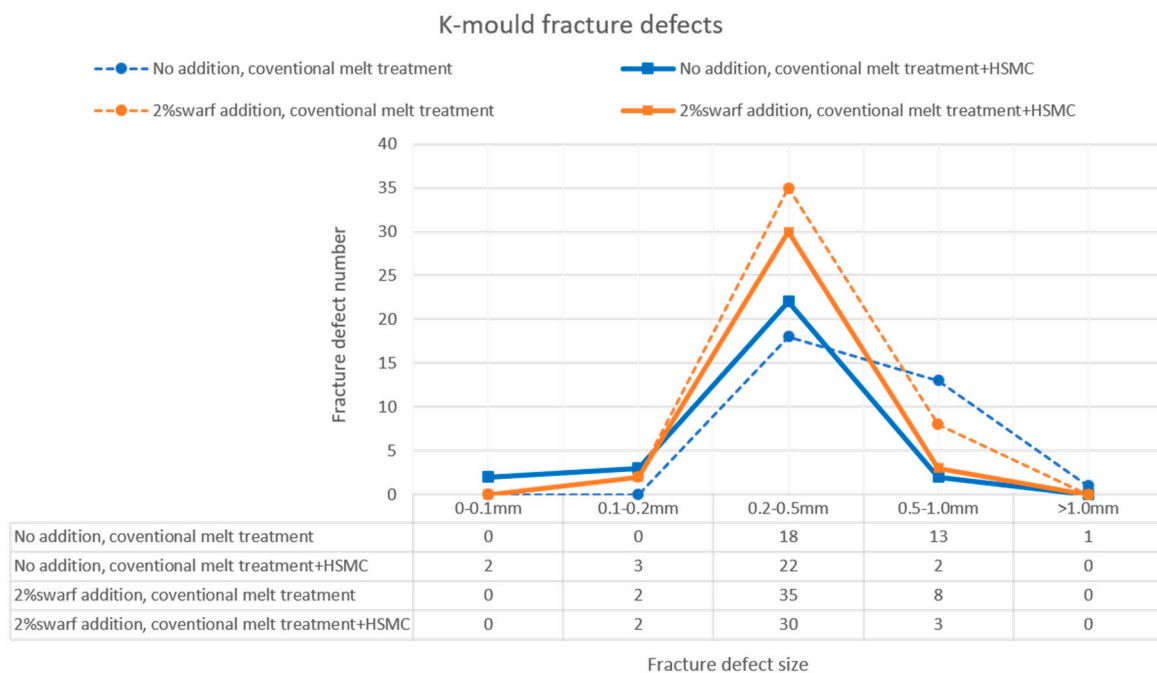


Figure 13. The effects of inclusions on the fracture defect size and distribution of the recycled A357 alloy before and after the melt treatment.

4. Discussion

4.1. Formation Mechanism of the Inclusions in the Recycled A357 Alloy

The recycling of aluminum alloys often increases the volume fraction of inclusions, which can adversely affect the castability of the material. The formation of inclusions in the recycled Al alloy was highly dependent on the conditions of the aluminum scrap. The major constituents of inclusions in aluminum melts have been found to be oxides, and the role of oxide films and particles in controlling the aluminum casting properties has been extensively researched over the last few decades [19]. It has been concluded that the number of pores, such as shrinkage and gas pores, and cracks are significantly affected by oxide films/oxide inclusions, which results in poor mechanical properties. In the recycled A357 alloys, old oxide films and young oxide films, which were identified by the different dimensions of the wrinkles and folds, along with the film thickness, indicating their formation at different stages, extensively accumulated. The old films were those that already existed in the previous recycled alloys or grew for a long period of time from a young film during the melt preparation, appearing as a lengthy curved feature. They typically had extremely large sizes and number densities and, therefore, were observed to be the most harmful inclusions. The young films formed due to the oxidation of the fresh melt when exposed to air during the melt treatment and pouring. The formed thin oxide layer easily folded and became entrapped in the melt by internal or external vibrations, which exposed the fresh melt to the air, forming a fresh oxide film again. These young oxide films had relatively small sizes and were usually less harmful compared to the older oxide films. However, continuous young films with a large number density of oxide particles may agglomerate together and grow into large oxide films, which normally cause large shrinkage defects during solidification. This phenomenon was found in the recycled A357 alloys with 2% swarf additions, as shown in Figure 7. The addition of swarf in this study represents an extreme case that leads to significant oxidation. It can be observed that the re-melting of swarf without a protective atmosphere increased the rate of oxidation and number of oxide films entrapped in the melt. During the melt holding, these entrapped new oxides either reacted and grew, eventually forming highly contoured double-oxide films characterized by convoluted cracks, identified as $MgAl_2O_4$ (Figure 7c), or remained as

Al₂O₃ films that agglomerated together on the micron scale (Figure 7d). They also appeared as thick oxide films surrounded by two new, non-wetting surface films.

When the partial pressure of oxygen is locally reduced because of the reaction between the melt and oxygen, nitrides have been reported to form because of the chemical reaction between the melt and atmosphere. The existence of AlN particles in the recycled A357 alloy aligns with Nyahumwa et al.'s hypothesis [20,21] that the consumption of the gases within the particular atmosphere of the bi-films results in the presence of nitrides in the casting process. As a result, the recycled A357 alloys with 2% swarf additions introduced large numbers of fresh oxide films; such a particular atmosphere trapped in the double-oxide film entrained in the melt promoted the formation of nitrides in the melt, which is shown in Figure 7.

Aluminum carbide inclusions have already been found as common inclusions in commercially pure aluminum ingots [19]. The re-melting of industrial scraps, especially with oil contaminations, will result in the presence of large carbon particles and further easily react with molten aluminum to precipitate aluminum carbide particles, which are detrimental to the mechanical properties. The 2% swarf addition in this research will have been contaminated with machining oil, therefore introducing more carbides due to the burning during the re-melting process. Moreover, aluminum carbide inclusions may also occur because of fairly long-term degassing of molten metal at high temperatures using a graphite impeller [21] or a reaction between molten aluminum and the unprotected surface of the crucibles with a deteriorated surface coating [22].

In the recycled aluminum alloys, the returned scraps are usually grain refined by Al–Ti–B master alloy and TiB₂ particles that always exist in the recycling of Al alloys. However, the TiB₂ particles were found to settle at the bottom of the melt and lost their effectiveness, as previously demonstrated [23,24]. This fading phenomenon becomes faster in melts with higher Si contents. Despite the relatively high residual concentrations of Ti and B in composition measurements, the effectiveness of TiB₂ particles is degraded by recycling. These residual TiB₂ particles are no longer present as grain refiner and gradually become inclusions. As a result, the extremely large number of TiB₂ particles found in the recycled A357 alloys in this research were mostly not performing as nucleating sites for grain refinement but present as harmful non-metallic inclusions that deteriorated the material's castability and mechanical properties.

4.2. Benefits of HSMC in Improving the Melt Quality of High Contaminated Recycled A357 Alloy

Generally, the ductility of cast aluminum alloys depends on factors such as defects, primary phase, secondary phase, and overall strength. However, the fracture behavior of the recycled A357 alloy, as observed from the K-mold results, is primarily attributed to the large defects, such as shrinkages, bi-oxides, and areas consisting of various inclusion particles. These defects are normally associated with inclusions and dissolved hydrogen in alloys. Because the hydrogen was controlled and measured to be similar for all of the melts, as shown in Figure 11, the defects observed in the microstructures were mainly the result of existing inclusions in the melts.

The microstructures of the recycled A357 alloys under various melt conditions, as shown in Figure 14, illustrate that the major defects in the cast samples were shrinkage porosities and continuous oxide films, along with various non-metallic inclusions. Macro- and micro-shrinkage porosities occur when the liquid metal is surrounded by significant amounts of solid materials, such as these oxide films and non-metallic inclusions, which are strong enough to resist the contraction of the liquid. They extensively occurred for the non-HSMC samples, as can be observed in Figure 14a. In addition, the size and number density of the abovementioned defects become larger when adding 2% swarf, as shown in Figure 14b. This confirms that the addition of swarf introduces more inclusions, increasing the likelihood of agglomeration and resulting in larger shrinkage defects. This is found to be extremely harmful to the material properties, especially for elongation, as it is well known that crack propagation easily starts from porosity defects [25]. After the formation of a crack

from oxide and porosity defects, the crack will propagate from the crack source to the whole fractured section. The decreased number and area fraction of the initial shrinkage and oxide defects in the recycled A357 alloy will be more efficient in impeding the propagation of the crack, which contributes to the increase in ductility as well. Thus, HSMC, as an effective method for dispersing inclusions and making them discontinuous converts them into a highly dispersed state to minimize their detrimental effects. It has, therefore, become a critical method for melt treatment and cleaning. As shown in the statistical results in Figure 14c,d, the percentage of the area of the shrinkage porosity defects decreased significantly, and the large continuous oxide inclusion defects were eliminated following the HSMC process. This means HSMC can affect the growth and final morphologies of these inclusions. With small particle sizes around one hundred nanometers and the small number density after being well-dispersed by HSMC, the inclusions in the melt had less harmful effects on the mechanical properties. As a result, the HSMC caused the existing inclusions to be less critical for the material's castability and has the potential to achieve a recycled A357 alloy with a better performance to facilitate the industrial recycling of aluminum alloys. Ongoing research work will focus on the effects of HSMC on the mechanical properties of recycled A357 alloys in real products as a next step.

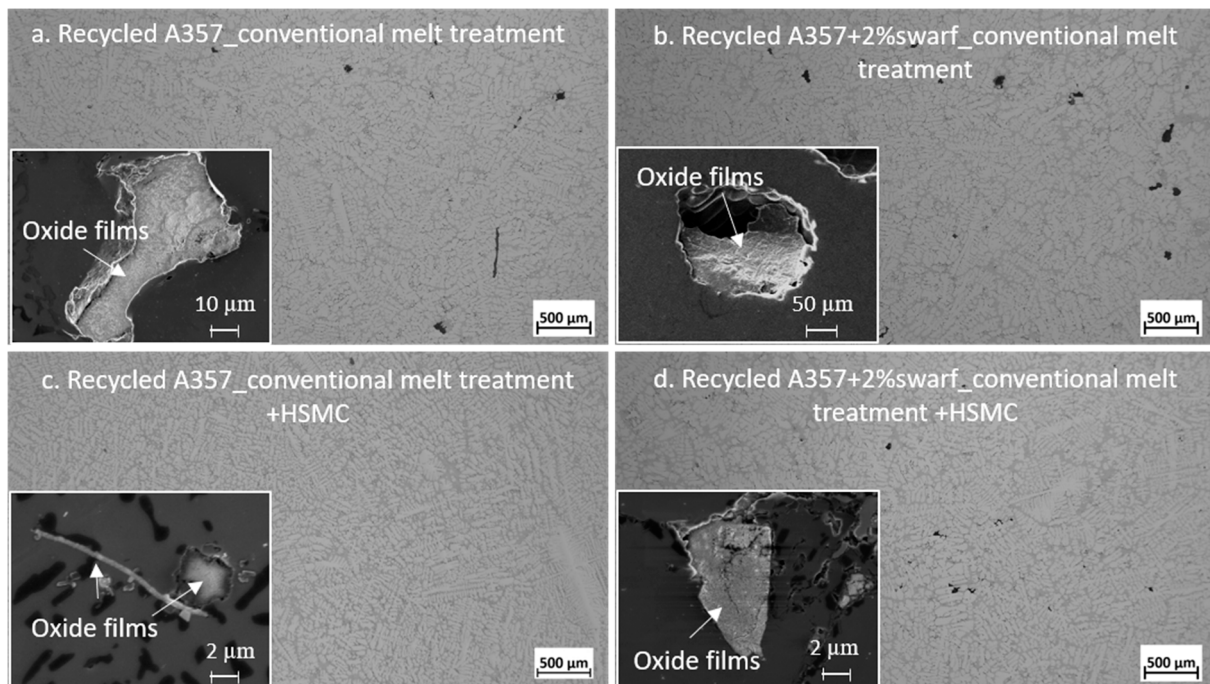


Figure 14. Microstructures of the recycled A357 alloys: (a) defects with large size in recycled A357 alloy with conventional melt treatment; (b) defects with large size and number density in recycled A357 alloy with 2% swarf addition with conventional melt treatment; (c) few defects in recycled A357 alloy under HSMC; (d) defects with smaller size and number density in recycled A357 alloy with 2% swarf addition under HSMC.

5. Conclusions

1. The predominant inclusions in the recycled A357 alloys consisted primarily of a significant amount of non-metallic inclusions, particularly TiB_2 particles and oxide films composed of discrete $MgAl_2O_4$ particles. Al_4C_3 , AlN , Ti-rich, and Fe-rich intermetallic compounds (IMCs) were also present as inclusions, although their number densities were relatively small.
2. Compared to the primary alloy, the inclusions identified in the recycled A357 alloy exhibited an extremely high number density and poor agglomeration, making them difficult to remove effectively from the melt using conventional degassing techniques.

The addition of swarf further exacerbated the size variation and increased the number density of the inclusions by introducing more fresh continuous oxides, carbide particles, and nitride films.

3. High shear melt conditioning (HSMC) technology was found to be an effective method for breaking up the agglomeration of entrapped inclusions, rendering them discontinuous and well-dispersed in the melt, thereby facilitating the removal of most large inclusions using conventional melt cleanliness techniques and converting the rest of the large inclusions into a highly dispersed state to minimize their detrimental effects.
4. The melt fluidity was restored to a higher value, and the size and number of the defects significantly decreased after the HSMC. The combination of HSMC technology with conventional melt treatment has the potential to enhance the melt condition before casting, resulting in noticeable improvements in the melt quality and material castability.

Author Contributions: Z.N., Experiments, Methodology, Writing, Reviewing, and Editing; Z.Q., Conceptualization, Methodology, Experiments, Writing, Reviewing, Editing, and Funding Acquisition; J.B.P., HSMC Technology Advice, Reviewing, and Editing; Z.F., Supervision. All authors have read and agreed to the published version of the manuscript.

Funding: This work was supported by the research project Circular Metals (EP/V011804/1) and by a Brunel University London BRIEF award (11937131).

Data Availability Statement: The original contributions presented in the study are included in the article, further inquiries can be directed to the corresponding authors.

Acknowledgments: We would like to thank Peter Lloyd for the HSMC technical support.

Conflicts of Interest: The authors declare no conflicts of interest.

References

1. Taub, A.I.; Krajewski, P.E.; Luo, A.A.; Owens, J.N. The evolution of technology for materials processing over the last 50 years: The automotive example. *JOM* **2007**, *59*, 48–57. [[CrossRef](#)]
2. Zhang, G.Z.; Wang, C.F.; Yin, S.; Teng, D.; Guan, R.G. Development of low-carbon energy storage material: Electrochemical behavior and discharge properties of iron-bearing Al-Li-based alloys as Al-air battery anodes. *J. Power Sources* **2023**, *585*, 233654. [[CrossRef](#)]
3. Mukhopadhyay, J.; Ramana, Y.V.; Singh, U. Extraction of Value Added Products from Aluminum Dross Material to Achieve Zero Waste. In *Proceedings of the Light Metals 2005: Proceedings of the Technical Sessions Presented by the TMS Aluminum Committee at the 134th TMS Annual Meeting, San Francisco, CA, USA, 13–17 February 2005*; pp. 1209–1212.
4. Das, S.K.; Green, J.A.S. The development of recycle-friendly automotive aluminum alloys. *JOM* **2007**, *59*, 47–51. [[CrossRef](#)]
5. Zhang, L.; Damoah, L.; Li, S.; Abebe, W. Mechanisms of Inclusion Removal from Aluminum through Filtration. In *Proceedings of the Light Metals 2008, Technical Session on Light Metals 2008 Held at the 137th TMS Annual Meeting, New Orleans, LA, USA, 9–13 March 2008*; pp. 649–655.
6. Gallo, R. “I Have Inclusions! Get Me the Cheapest and Best Flux for Cleaning My Melt!”—Is This the Best Driven, Cost-Saving Approach by a Foundry? In *Proceedings of the 121st Metal casting Congress of the American Foundry Society, Milwaukee, WI, USA, 25–27 April 2017*; pp. 17–105.
7. Gesing, A. Assuring the continued recycling of light metals in end-of-life vehicles: A global perspective. *J. Mater.* **2004**, *56*, 18–27. [[CrossRef](#)]
8. Gaustad, G.; Olivetti, E.; Kirchain, R. Improving aluminum recycling: A survey of sorting and impurity removal technologies. *Resour. Conserv. Recycl.* **2012**, *58*, 79–87. [[CrossRef](#)]
9. Ashtari, P.; Gerard, T.K.; Sadayappan, K. Removal of iron from recycled aluminum alloys. *Can. Metall. Q.* **2012**, *51*, 75–80. [[CrossRef](#)]
10. Campbell, J. *Castings*, 2nd ed.; Elsevier: Oxford, UK, 2003.
11. Alimi, S.A. Recycling aluminum for sustainable development: A review of different processing technologies in green manufacturing. *Results Eng.* **2024**, *23*, 102566. [[CrossRef](#)]
12. Cabrera, N.; Mott, N.F.; Wills, H.H. Theory of the Oxidation of Metals. *Rep. Prog. Phys.* **1949**, *12*, 163–184. [[CrossRef](#)]
13. Schultze, J.W.; Lohrengel, M.M. Stability, reactivity and breakdown of passive films. Problems of recent and future research. *Electrochim. Acta* **2000**, *45*, 2499–2513. [[CrossRef](#)]

14. Cao, X.; Campbell, J. A critical review of techniques for the removal of oxide films (including the heat treatment of liquid metal). In Proceedings of the 2nd International Aluminum Casting Technology Symposium, Columbus, OH, USA, 7–9 October 2002; pp. 135–146.
15. Fan, Z.; Zuo, Y.B.; Jiang, B. Apparatus and Method for Liquid Metals Treatment. WO Patent 2012035357 A1, 22 March 2012.
16. Patel, J.B.; Yang, X.; Mendis, C.L.; Fan, Z. Melt Conditioning of Light Metals by Application of High Shear for Improved Microstructure and Defect Control. *JOM* **2017**, *69*, 1071–1076. [[CrossRef](#)] [[PubMed](#)]
17. Jaime, L.N.; Patel, J.B.; Fan, Z. Improved degassing efficiency and mechanical properties of A356 aluminum alloy castings by high shear melt conditioning (HSMC) technology. *J. Mater. Process. Technol.* **2021**, *294*, 117146.
18. Niu, Z.; Wang, S.; Gao, F.; Fan, Z. Nature of Oxides in Al–Mg Alloys. *Trans. Indian. Inst. Met.* **2024**, *77*, 2929–2933. [[CrossRef](#)]
19. Simensen, C.J.; Berg, C. A Survey of Inclusions in Aluminum. *Alum. Dusseld.* **1980**, *56*, 335–340.
20. Nyahumwa, C.; Green, N.R.; Campbell, J. Effect of Mold-Filling Turbulence on the Fatigue Properties of Cast Aluminum Alloys. *AFS Trans.* **1998**, *106*, 215–223.
21. Raiszadeh, R.; Griffiths, W.D. A method to study the history of a double oxide film defect in liquid aluminum alloys. *Metall. Mater. Trans. B* **2006**, *37*, 865–871. [[CrossRef](#)]
22. Lloyed, D.J.; Lagace, H.; McLeod, A.; Morris, P.L. Microstructural aspects of aluminum-silicon carbide particulate composites produced by a casting method. *Mater. Sci. Eng. A* **1989**, *107*, 73–80. [[CrossRef](#)]
23. Limmaneevichitr, C.; Eidhed, W. Fading mechanism of grain refinement of aluminum–silicon alloy with Al–Ti–B grain refiners. *Mater. Sci. Eng. A* **2003**, *349*, 197–206. [[CrossRef](#)]
24. Limmaneevichitr, C.; Eidhed, W.; Eisuke, N. Effects of Residual TiB₂ and TiAl₃ Nucleant on Grain-Refinement of Recycled Aluminum-Silicon Alloy Castings. In Proceedings of the 9th International Conference on Aluminum Alloys, Brisbane, Australian, 2 August 2004; pp. 576–581.
25. Dong, X.X.; He, L.J.; Huang, X.S.; Li, P.J. Effect of electromagnetic transport process on the improvement of hydrogen porosity defect in A380 aluminum alloy. *Int. J. Hydrogen Energy* **2015**, *40*, 9287–9297. [[CrossRef](#)]

Disclaimer/Publisher’s Note: The statements, opinions and data contained in all publications are solely those of the individual author(s) and contributor(s) and not of MDPI and/or the editor(s). MDPI and/or the editor(s) disclaim responsibility for any injury to people or property resulting from any ideas, methods, instructions or products referred to in the content.